mained completely stationary in space, but still exhibited intensity fluctuations of up to 40%. Because individual small fluorophores locked in the gel matrix yielded stable intensities (Fig. 3), we tentatively interpret these amplitude fluctuations as resulting from slow orientational changes of the fluorophore relative to the laser polarization. The motion of the fluorophore label is likely to be hindered by the gel matrix and the nearby protein conformation.

Our experiments indicate that PAA gels offer promise as hosts for single-molecule studies of biological systems. Ease of preparation and controllable pore size make this host material a particularly flexible matrix that should facilitate the study of singly labeled proteins, electrophoresis (*29*), and individual reactions in solutions. For small fluorophores like nile red, gels as hosts hinder the distance traveled as a result of Brownian motion by approximately two orders of magnitude in each direction for observations on the order of 1 s. This observation means that the signal from any one solvated molecule is concentrated in 1/10,000th of the area of a similar molecule in free solution, thus providing a large increase in detectability solely from the use of the PAA matrix. Although biased in the axial direction, the use of the evanescent field generated by TIR has yielded 3D trajectories of single molecules in solution (*30*).

REFERENCES AND NOTES

1. W. E. Moerner and L. Kador, *Phys. Rev. Lett.* **62**, 2535 (1989).
2. M. Orrit and J. Bernard, *ibid.* **65**, 2716 (1990).
3. For a review, see W. E. Moerner, *Science* **265**, 46 (1994).
4. E. B. Shera, N. K. Seitzinger, L. M. Davis, R. A. Keller, S. A. Soper, *Chem. Phys. Lett.* **174**, 553 (1990).
5. C. W. Wilkerson, P. M. Goodwin, W. P. Ambrose, J. C. Martin, R. A. Keller, *Appl. Phys. Lett.* **62**, 2030 (1993).
6. M. Eigen and R. Rigler, *Proc. Natl. Acad. Sci. U.S.A.* **91**, 5740 (1994).
7. S. Nie, D. T. Chiu, R. N. Zare, *Science* **266**, 1018 (1994).
8. B. B. Haab and R. A. Mathies, *Anal. Chem.* **67**, 3253 (1995).
9. F. Guttler, T. Irngartinger, T. Plakhotnik, A. Renn, U. P. Wild, *Chem. Phys. Lett.* **217**, 393 (1994); J. Jasny *et al.*, *Rev. Sci. Instrum.* **67**, 1425 (1996).
10. Th. Schmidt, G. J. Schutz, W. Baumgartner, H. J. Gruber, H. Schindler, *Proc. Natl. Acad. Sci. U.S.A.* **93**, 2926 (1996).
11. T. Ha *et al.*, *ibid.*, p. 6264.
12. E. Betzig and R. J. Chichester, *Science* **262**, 1422 (1993).
13. J. K. Trautman, J. J. Macklin, L. E. Brus, E. Betzig, *Nature* **369**, 40 (1994).
14. W. P. Ambrose, P. M. Goodwin, J. C. Martin, R. A. Keller, *Science* **265**, 364 (1994).
15. X. S. Xie and R. C. Dunn, *ibid.*, p. 361.
16. J. J. Macklin, J. K. Trautman, T. D. Harris, L. E. Brus, *ibid.* **272**, 255 (1996).
17. J. K. Trautman and J. J. Macklin, *Chem. Phys.* **205**, 221 (1996).
18. A. J. Meixner, D. Zeisel, M. A. Bopp, G. Tarrach, *Opt. Eng.* **34**, 2324 (1995).
19. T. Funatsu, Y. Harada, M. Tokunaga, K. Saito, T. Yanagida, *Nature* **374**, 555 (1995); R. D. Vale *et al.*, *ibid.* **380**, 451 (1996).
20. J. S. Fawcett and C. J. O. R. Morris, *Sep. Sci.* **1**, 9 (1966).
21. A. G. Ogston, *Trans. Faraday Soc.* **54**, 1754 (1958).
22. D. Rodbard, in *Methods of Protein Separation*, N. Catsimpoolas, Ed. (Plenum, New York, 1976), vol. 2, pp. 145–218.
23. B. D. Hames and D. Rickwood, Eds., *Gel Electrophoresis of Proteins: A Practical Approach*, (Oxford Univ. Press, New York, ed. 2, 1990).
24. J.-R. Daban, M. Samso, S. Bartolome, *Anal. Biochem.* **199**, 162 (1991); *ibid.*, p. 169.
25. J. D. Jackson, *Classical Electrodynamics* (Wiley, New York, 1975), p. 283.
26. B. J. Berne and R. Pecora, *Dynamic Light Scattering with Applications to Chemistry, Biology, and Physics* (Krieger, Malabar, FL, 1990), pp. 143–149.
27. At a glass/solution boundary, this approximation holds to within 10%; the slight deviation from exponentiality arises from near-field coupling of the dipole radiation into the more optically dense glass. See, for example, D. Axelrod and E. H. Hellen, in *Fluorescence Microscopy of Living Cells in Culture, Part B*, D. L. Taylor and Y.-L. Wang, Eds. (Academic Press, San Diego, CA, 1989), pp. 399–416.
28. A. Feinstein and A. J. Rowe, *Nature* **205**, 147 (1965).
29. B. H. Zimm and O. Lumpkin, *Macromolecules* **26**, 226 (1993).
30. Assuming a Gaussian distribution of molecular displacements, the mean-square axial displacement, $\langle z^2 \rangle$, should be equal to $\langle x^2 \rangle$ and $\langle y^2 \rangle$. To correct for the axial bias, we recall that ~2% of the molecules were observed to be in at least four successive frames. Measured $\langle z^2 \rangle$ values for several of these molecules were $\sim 2 \times 10^{-3}$ μm². The probability of an axial mean square displacement this small occurring in the distributions defined by the measured $\langle x^2 \rangle$ and $\langle y^2 \rangle$ values (Table 1) is ~2.7%, thus indicating that, within our experimental error, diffusion in axial and transverse directions is equivalent.
31. We thank L. S. B. Goldstein and R. Sakowicz for useful discussions and for the Cy5-labeled antibody, and B. H. Zimm for a critical reading of the manuscript. D. J. N. was supported in part by a National Science Foundation Postdoctoral Fellowship.

29 July 1996; accepted 18 September 1996

Rate Constants for Charge Transfer Across Semiconductor-Liquid Interfaces

Arnel M. Fajardo and Nathan S. Lewis*

Interfacial charge-transfer rate constants have been measured for *n*-type Si electrodes in contact with a series of viologen-based redox couples in methanol through analyses of the behavior of these junctions with respect to their current density versus potential and differential capacitance versus potential properties. The data allow evaluation of the maximum rate constant (and therefore the electronic coupling) for majority carriers in the solid as well as of the dependence of the rate constant on the driving force for transfer of delocalized electrons from the *n*-Si semiconducting electrode into the localized molecular redox species in the solution phase. The data are in good agreement with existing models of this interfacial electron transfer process and provide insight into the fundamental kinetic events underlying the use of semiconducting photoelectrodes in applications such as solar energy conversion.

Charge-transfer rate constants from delocalized carriers in a semiconducting electrode to outer-sphere redox systems in a liquid electrolyte are an important, controversial, and relatively unexplored aspect of photoelectrochemical energy conversion devices (*1–7*). The kinetic behavior of the delocalized electron in the solid transferring to an electron acceptor in the solution phase is a key issue that is not as fully understood as the process of charge transfer between molecular donors and acceptors in the photosynthetic process (*8*) and related model systems (*9*). Research has recently focused on the magnitude of the electronic coupling terms of these interfacial processes, because such quantities are required to estimate the maximum charge-transfer rate constant expected under conditions of optimal exoergicity (*2, 6, 10–12*). Very large charge-transfer rate constants of majority carriers in the semiconductor can lead to substantial levels of recombination and efficiency losses in photoelectrochemical energy conversion devices, whereas very small interfacial rate constants would be undesirable because they could prevent efficient collection of photogenerated minority charge carriers by redox ions in the solution. Experimental measurements of these rate constants have largely been thwarted by the nonideal energetic behavior of stable semiconductor-liquid contacts (*1*) and by the lack of reliable kinetic measurements on stable semiconductor electrodes in contact with outer-sphere redox couples (*2*). Here, we describe measurements of charge-transfer rate constants for *n*-type Si electrodes in contact with a series of viologen acceptors. These data have yielded experimental values for the maximum majority carrier charge-transfer rate constant at optimal exoergicity and for the reorganization energy for charge transfer across these solid-liquid junctions.

Single-crystal, (100)-oriented *n*-Si electrodes with donor densities N_d of either 7.84×10^{14} or 6.95×10^{15} cm^{-3} were used in

---

Division of Chemistry and Chemical Engineering, California Institute of Technology, Pasadena, CA 91125, USA.

*To whom correspondence should be addressed.

this study. The electrodes were etched in 48% aqueous HF and rinsed with CH_3OH, and the subsequent electrochemistry was performed in an anaerobic atmosphere with standard drybox methods to prevent oxidation of the Si surface (*13*). Electrochemical methods and instrumentation were as described previously (*10*), and all of the redox couples were synthesized and purified according to published procedures (*14*). The electrolyte in all cells was 1.0 M LiCl.

The desired interfacial charge-transfer rate constant is expected to be bimolecular—that is, first order in the concentration of electrons at the semiconductor surface n_s and first order in the concentration of electron acceptors in the interphase region of the electrolyte [A] (*2*, *3*). Hence, to extract reliably the desired charge-transfer rate constant from steady-state current density (*J*)–potential (*E*) measurements, two criteria must be met: The interfacial energetics must be known so that the bulk electron concentration can be related to n_s, and the measured *J* must be linearly dependent on both n_s and [A]. As described below, the systems we studied satisfy these two criteria. Thus, the desired rate constant k_{et} is readily extracted from the data, because $k_{et} = J/(qn_s[A])$, where *q* is the electronic charge and the other quantities are determined experimentally.

The energetics of the various Si-CH_3OH contacts were determined by measurement of differential capacitance versus potential. In this well-known technique, the reciprocal of the square of the differential capacitance of the semiconductor, C_{sc}, should be linearly related to the electrode potential and should be independent of the measurement frequency (*3*, *15*). Although frequency-dependent C_{sc} behavior has generally been reported for semiconductor electrodes in contact with nonaqueous solvents (*16*), which makes extraction of the desired energetic parameters problematic, careful attention to various experimental factors (including maximizing the electrode area/perimeter ratio and minimizing the frequency dispersion due to the potentiostat and counterelectrode) allowed experimental realization of this ideally expected behavior (Fig. 1). The C_{sc}^{-2} versus *E* data for *n*-Si electrodes in contact with two representative redox systems, benzyl viologen$^{2+/+}$ and 1,1′-bis(diethoxycarbonylmethyl)-4,4′-bipyridinium$^{2+/+}$, are shown in Fig. 1, B and C. The data were independent of frequency from 2.5 to 100 kHz (that is, log-log plots of the magnitude of impedance versus frequency at various potentials in reverse bias were linear, with slopes of −1.00 from 10^3 to 10^5 Hz; Fig. 1A), and the slope of the best-fit line through the C_{sc}^{-2} versus *E* data was within 10% of the value expected from the known dopant density of the electrodes. The intercept yielded the flat-band potential E_{fb}, which was then used to measure the driving force for the interfacial electron transfer event ΔG°′, with

$$\Delta G^{\circ\prime} = qE_{fb} - kT\ln(N_c/N_d) - qE^{\circ\prime}(A/A^-) \quad (1)$$

where $E^{\circ\prime}(A/A^-)$ is the formal reduction potential of the solution, N_c is the effective density of states in the semiconductor conduction band, *k* is the Boltzmann constant, and *T* is the cell temperature. E_{fb} was also used to relate n_s to N_d at the various electrode potentials of interest in the kinetic measurements through the Boltzmann relation

$$n_s = N_d \exp[-q(E - E_{fb})/kT] \quad (2)$$

(*3*, *15*). Although the redox potentials of the solutions we used varied by >400 mV, the Si electrode showed ideal energetic behavior (*4*) in that the conduction band edge energy remained constant at −0.92 V versus the saturated calomel electrode (SCE) for the entire range of viologen systems.

The representative kinetic behavior of these Si-liquid contacts is shown in Fig. 2.

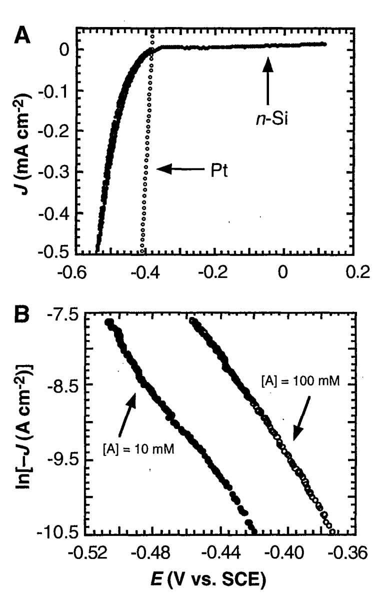

Fig. 2. *J*-*E* characteristics, corrected for solution resistance and concentration overpotentials, for the *n*-Si-CH_3OH–benzyl viologen$^{2+/+}$ interface. The specifications of the *n*-Si electrode are the same as those in Fig. 1. (**A**) A comparison of the *J*-*E* behavior of a 1.1-cm^2 Pt electrode and that of an *n*-Si electrode in contact with CH_3OH–benzyl viologen^{2+} (10 mM)–benzyl viologen^{+} (10 mM). The increased polarization required at the semiconductor electrode to produce the same current density as at the Pt electrode indicates that the currents of the Si-liquid contact are limited primarily by interfacial charge-transfer kinetics and not by mass transport nor by concentration overpotentials. (**B**) The shift in *J* of an *n*-Si electrode as the concentration of electron acceptor [A] is increased (with [A^-] held constant at 10 mM) and as the electrode potential is varied indicates a first-order kinetic dependence of the interfacial flux on both the acceptor concentration and the electron concentration at the surface of the semiconductor. Linear regression of ln *J* versus *E* yielded slopes of 68.6 ± 0.5 (correlation coefficient $R = 0.997$) and 65.0 ± 0.3 mV ($R = 0.999$) per decade of *J* for the data displayed with [A] = 10 mM and 100 mM, respectively.

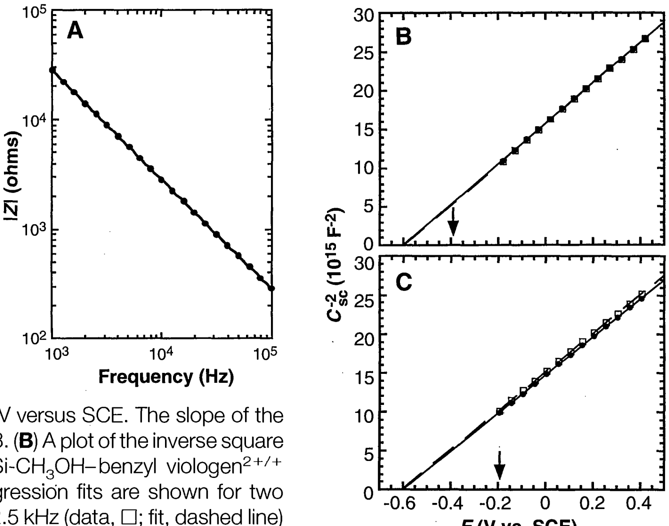

Fig. 1. Impedance characteristics of an *n*-Si electrode with a measured dopant density of 7.84 × 10^{14} cm^{-3} and a photographic area of 0.83 cm^2. (**A**) A representative Bode plot (logarithm of the magnitude of the impedance |*Z*| versus logarithm of the measurement frequency) of the *n*-Si-CH_3OH–benzyl viologen^{2+} (10 mM)–benzyl viologen^{+} (10 mM) contact at an applied potential of +0.418 V versus SCE. The slope of the linear regression was −0.998. (**B**) A plot of the inverse square of C_{sc} versus *E* for the *n*-Si-CH_3OH–benzyl viologen$^{2+/+}$ contact. Data and linear regression fits are shown for two representative frequencies, 2.5 kHz (data, □; fit, dashed line) and 100 kHz (data, ●; fit, solid line). Over this frequency range, the *x*-intercept changed by 5 mV and averaged −0.603 V versus SCE. The arrow signifies the solution potential of −0.382 V versus SCE. (**C**) A plot of C_{sc}^{-2} versus *E* for the *n*-Si-CH_3OH–1,1′-bis(diethoxycarbonylmethyl)-4,4′-bipyridinium$^{2+/+}$ contact. Over the same frequency range given in (B), the *x*-intercept changed by 6 mV and averaged −0.601 V versus SCE. The solution potential, marked by the arrow, was −0.195 V versus SCE. Standard deviations in the value of E_{fb} over a number of trials on various Si-CH_3OH contacts were ~20 mV.

In each case, the *J-E* data exhibited rectification to anodic current flow, with

$$J = -J_o(\exp\{-q[E - E(A/A^-)]/\gamma kT\} - 1) \quad (3)$$

where J_o is the exchange current density of the semiconductor-liquid contact, $E(A/A^-)$ is the Nernst potential of the solution, and γ is the diode quality factor. The data clearly reflected kinetic limitations to charge transfer at the semiconductor-liquid contact because the current density observed at a potential of the Si electrode was far lower than that observed at the same potential of a Pt electrode in the same electrolyte solution (Fig. 2A). After correction for series resistance and concentration overpotentials (*17*), the current density of the Si electrodes displayed a linear dependence of ln *J* versus *E* in the forward bias (cathodic current) region, with a slope of 66 ± 14 mV (1σ standard deviation over 22 trials) per decade of current density (Fig. 2B). This result verifies that the charge-transfer event is linearly dependent on n_s with a slope close to the theoretically expected value of 59 mV per decade of current density (*4*). The data in Fig. 2B also show the expected dependence of *J* on the acceptor concentration; when [A] was increased, the *J* at a given potential increased. The potential shift in the *J-E* behavior is expected to be 59 mV for a 10-fold increase in [A] (*3*), and the data typically showed shifts of 55 to 62 mV per decade of [A] for all of the redox couples we studied. Because of these nearly ideal dependences, the k_{et} values deduced from the data were essentially independent of the *E* and [A] values chosen for evaluation, with any variation incorporated into the error bars of the quoted k_{et} result (Fig. 3). These error bars also incorporate the errors of the C_{sc}^{-2} versus *E* data in assigning E_{fb} and therefore in calculating n_s. All rate measurements were performed at potentials at which *J* far exceeded J_o to ensure that the rate of electron injection from the solution into the semiconductor was negligible compared with the rate of electron transfer from the solid into the electrolyte. A value of $k_{et} = (6 \pm 3) \times 10^{17}$ cm^4 s^{-1} is obtained from the data of Figs. 1 and 2 for the Si-CH$_3$OH–benzyl viologen$^{2+/+}$ contact.

The k_{et} data for various Si-CH$_3$OH–viologen$^{2+/+}$ contacts, plotted as k_{et} versus $\Delta G^{\circ\prime}$ (*18*), are compiled in Fig. 3. The data show a value of $k_{et,max}$ of $\sim 6 \times 10^{-17}$ cm^4 s^{-1}. This maximum value for k_{et} is in excellent accord with the predictions of a working model for estimating such rate constants (*2, 10, 19*). In addition, our data are incompatible with suggestions that $k_{et,max}$ for majority carrier transfer is in general $>10^{-14}$ cm^4 s^{-1} and is perhaps as large as 10^{-12} cm^4 s^{-1} (*6, 12, 20*). The data thus indicate that the effective capture cross section of the outer-sphere redox acceptors studied here is close to their geometric cross section, as expected for an off-resonance event (*2*). The reorganization energy λ deduced from a fit of the data of Fig. 3 to the classical parabolic Marcus relation is approximately 0.6 to 0.7 eV, which is in reasonable agreement with the value of 0.50 eV calculated for methyl viologen^{2+} in CH$_3$OH from electron self-exchange rate constant measurements (*21*). The value of λ for this ion indicated by the data of Fig. 3—a somewhat larger value than is predicted at a metal-electrolyte interface (*22*)—could arise from some reorganization of the solvent around the surface electrons, from a loss of the image charge stabilization [that should lower λ for ions in direct or near contact with a metallic electrode surface (*23*)], or from another source. Learning more about the generality and origin of this effect will require further kinetic data on related semiconductor-liquid contacts.

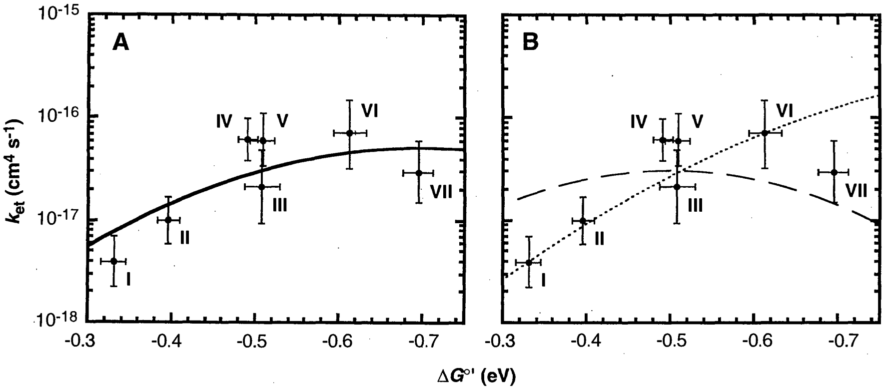

Fig. 3. Plots of the electron transfer rate constant k_{et} as a function of the driving force for the charge-transfer event $\Delta G^{\circ\prime}$. The redox systems were 7,8-dihydro-6*H*-dipyrido[1,2-a:2′,1′-c]-[1,4]-diazepinium$^{2+/+}$ (**I**), 6,7-dihydro-2,11-dimethyldipyrido[1,2-a:2′,1′-c]pyrazinium$^{2+/+}$ (**II**), 6,7-dihydro-dipyrido[1,2-a:2′,1′-c]pyrazinium$^{2+/+}$ (**III**), methyl viologen$^{2+/+}$ (**IV**), benzyl viologen$^{2+/+}$ (**V**), 1,1′-bis-(ethoxycarbonylmethyl)-4,4′-bipyridinium$^{2+/+}$ (**VI**), and 1,1′-bis(diethoxycarbonylmethyl)-4,4′-bipyridinium$^{2+/+}$ (**VII**). The errors in the rate constant determination (vertical error bars) arose mostly from errors associated with determination of the surface electron concentration, which is exponentially dependent on the experimentally determined E_{fb} (whose error is reflected in the horizontal error bars). (**A**) The solid curve depicts the behavior expected from the classical Marcus theory description of such electron transfer events, using $k_{et,max} = 5.0 \times 10^{-17}$ cm^4 s^{-1} and $\lambda = 0.70$ eV. (**B**) The dashed curve illustrates a fit to the predictions of classical Marcus theory for $\lambda = 0.50$ eV (which required adjusting $k_{et,max}$ to 3.0×10^{-17} cm^4 s^{-1}), whereas the dotted curve shows a Marcus fit to $\lambda = 1.0$ eV (which required adjusting $k_{et,max}$ to 3.0×10^{-16} cm^4 s^{-1}). The lack of a good fit produced by these parameters illustrates the limited range of λ (and $k_{et,max}$) that is compatible with the data.

REFERENCES AND NOTES

1. C. A. Koval and J. N. Howard, *Chem. Rev.* **92**, 411 (1992).
2. N. S. Lewis, *Annu. Rev. Phys. Chem.* **42**, 543 (1991).
3. S. R. Morrison, *Electrochemistry at Semiconductor and Oxidized Metal Electrodes* (Plenum, New York, 1980).
4. H. O. Finklea, *Semiconductor Electrodes*, vol. 55 of *Studies in Physical and Theoretical Chemistry* (Elsevier, New York, 1988).
5. A. J. Nozik, Ed., *Photoeffects at Semiconductor-Electrolyte Interfaces*, vol. 146 of *ACS Symposium Series* (American Chemical Society, Washington, DC, 1981); R. Memming, in *Electrochemistry II*, vol. 143 of *Topics in Current Chemistry*, E. Steckhan, Ed. (Springer-Verlag, New York, 1988), pp. 79–112; L. M. Peter, in *Electrochemistry*, D. Pletcher, Ed. (Royal Society of Chemistry, London, 1984), pp. 66–100.
6. B. B. Smith and A. J. Nozik, *Chem. Phys.* **205**, 47 (1996); B. B. Smith, J. W. Halley, A. J. Nozik, *ibid.*, p. 245.
7. I. Uhlendorf, R. Reinekekoch, R. Memming, *J. Phys. Chem.* **100**, 4930 (1996); B. R. Horrocks, M. V. Mirkin, A. J. Bard, *ibid.* **98**, 9106 (1994).
8. J. Deisenhofer and J. R. Norris Jr., Eds., *The Photosynthetic Reaction Center* (Academic Press, San Diego, CA, 1993).
9. G. L. Closs and J. R. Miller, *Science* **240**, 440 (1988); B. E. Bowler, A. L. Raphael, H. B. Gray, *Prog. Inorg. Chem.* **38**, 259 (1990).
10. K. E. Pomykal, A. M. Fajardo, N. S. Lewis, *J. Phys. Chem.* **100**, 3652 (1996).
11. J. N. Howard and C. A. Koval, *Anal. Chem.* **66**, 4525 (1994); H. Gerischer, *J. Phys. Chem.* **95**, 1356 (1991).
12. Y. Rosenwaks *et al.*, *J. Phys. Chem.* **98**, 2739 (1994).
13. After electrochemistry, no oxidation in the Si 2*p* region was detected with high-resolution x-ray photoelectron spectroscopy; the signals showed only the expected substrate Si 2*p* doublet at 99.8 eV binding energy.
14. R. F. Homer and T. E. Tomlinson, *J. Chem. Soc.* **1960**, 2498 (1960); S. Hünig and W. Schenk, *Liebigs Ann. Chem.* **1979**, 727 (1979).
15. S. M. Sze, *The Physics of Semiconductor Devices* (Wiley, New York, 1981).
16. M. Tomkiewicz, *Electrochim. Acta* **35**, 1631 (1990); H. Kobayashi, N. Takeda, H. Sugahara, H. Tsubomura, *J. Phys. Chem.* **95**, 813 (1991); G. Nagasubramanian, B. L. Wheeler, F.-R. F. Fan, A. J. Bard, *J. Electrochem. Soc.* **129**, 1742 (1982); G. Nagasubramanian, B. L. Wheeler, A. J. Bard, *ibid.* **130**, 1680 (1983); G. Nagasubramanian, B. L. Wheeler, G. A. Hope, A. J. Bard, *ibid.*, p. 385.
17. A. J. Bard and L. R. Faulkner, *Electrochemical Methods: Fundamentals and Applications* (Wiley, New York, 1980). Mass transport limitations were determined with a Pt working electrode in the same cell geometry as the Si electrode. The small correction of the observed *J-E*

data for concentration polarization at each measurement potential was performed according to conventional procedures, and this correction was incorporated into the *J-E* data of Fig. 2B. No correction was made for double-layer effects on the rate constant, although the ions being reduced were dipositively charged. This correction is extremely small for a semiconductor-liquid interface because at the electrolyte concentration we used, the differential capacitance of the semiconductor is about one-thousandth that of the Helmholtz layer (compare with Fig. 1). The Frumkin correction that relates the bulk and surface concentrations of a redox-active ion in the solution is negligible under such experimental conditions (W. J. Royea, O. Krüger, N. S. Lewis, in preparation).

18. Further variation in driving force was precluded at negative potentials, because of the formation of nonrectifying junctions, and in the positive region, because of the change in the rate-limiting step to bulk recombination-diffusion [M. L. Rosenbluth and N. S. Lewis, *J. Am. Chem. Soc.* **108**, 4689 (1986)]. The rate constants determined here primarily reflect the conduction-band kinetic process because the valence band process of Si-CH_3OH–dimethylferrocene$^{+/0}$ contacts, which was identified as bulk recombination-diffusion in this small band-gap semiconductor, exhibits a different dependence of J on [A]. In addition, the use of ohmic-selective contacts has shown directly that the J in the systems described here is associated with electron transfer from the conduction band as opposed to hole transfer into the valence band [M. X. Tan, C. N. Kenyon, N. S. Lewis, *J. Phys. Chem.* **98**, 4959 (1994)].
19. Morrison has reported rate constant values of 10^{-20} to 10^{-15} cm^4 s^{-1} for electron transfer from ZnO to various acceptors in aqueous solution [S. R. Morrison, *Surf. Sci.* **15**, 363 (1969); ______ and T. Freund, *ibid.* **9**, 119 (1968)]. A $k_{et,max}$ of 10^{-16} cm^4 s^{-1} was suggested by the trend of the observed capture cross section versus standard reduction potential, although the variation of λ by >1 eV for the series of acceptors used precludes a quantitative evaluation of the generality of this observation. In addition, the anomalously steep decline in rate constant observed at high exoergicity, along with an anomalous pH dependence of the rate constant for reduction of aqueous $Fe(CN)_6{}^{3-}$, led these authors to suggest a strong role for inner-sphere electron transfer, adsorption processes, or both in these kinetic events. Our rate constant data are in qualitative agreement with the value of $k_{et,max}$ suggested by these authors, although such agreement might well be fortuitous.
20. Y. Rosenwaks, B. R. Thacker, R. K. Ahrenkiel, A. J. Nozik, *J. Phys. Chem.* **96**, 10096 (1992).
21. S. Dai, thesis, University of Tennessee, Knoxville (1990); F. Williams, *U.S. Dep. Energy Rep. 91015008* (1991).
22. R. A. Marcus, *J. Chem. Phys.* **43**, 679 (1965).
23. B. B. Smith and C. A. Koval, *J. Electroanal. Chem.* **277**, 43 (1990).
24. Supported by NSF grant CHE-9634152.

25 June 1996; accepted 13 September 1996

Maturation of a Central Glutamatergic Synapse

G.-Y. Wu, R. Malinow, H. T. Cline*

Whole-cell recordings from optic tectal neurons in *Xenopus* tadpoles were used to study the maturation of a glutamatergic synapse. The first glutamatergic transmission is mediated only by *N*-methyl-D-aspartate (NMDA) receptors and is silent at resting potentials. More mature synapses acquire transmission by α-amino-3-hydroxy-5-methyl-4-isoxazole propionic acid (AMPA) receptors. This maturational program is mimicked by postsynaptic expression of constitutively active calcium-calmodulin–dependent protein kinase II (CaMKII). Newly formed synapses may be silent unless sufficient depolarization is provided by coincident activity that could activate postsynaptic CaMKII, resulting in the appearance of AMPA responses.

Most excitatory synapses in the vertebrate central nervous system use glutamate to mediate synaptic transmission (*1*) through two types of ionotropic receptors, the AMPA and NMDA receptors. AMPA and NMDA receptors are distinguishable by their pharmacological and biophysical properties (*2*). In particular, at hyperpolarized potentials, NMDA receptor channels are to a large extent blocked by Mg^{2+}, whereas AMPA receptors are capable of transmission. Although a single neuron may express both receptors (*3*), their distribution at individual synapses is less clear (*4*, *5*). Recent studies have suggested that many synapses in early postnatal hippocampus have only functional NMDA receptors (*6–9*). A wide spectrum of developmental stages can be studied in a single tadpole optic tectum because neurons are in different developmental stages along the rostrocaudal (RC) axis (*10*). We investigated the physiological properties of early synaptic development in this system and examined whether retinotectal synapses initially transmit with only NMDA receptors and add an AMPA component with maturation.

We also investigated the role of the calcium-calmodulin–dependent protein kinase II (CaMKII) in synaptic maturation. The expression of this enzyme is developmentally regulated (*11*), is concentrated in synaptic regions (*12*, *13*), and has been implicated in control of neuronal growth and synaptogenesis (*14–16*), as well as in activity-dependent synaptic plasticity (*17–21*). To determine whether CaMKII activity is sufficient to cause maturation of glutamatergic synapses, we increased CaMKII activity specifically in postsynaptic tectal neurons, and not in the presynaptic retinal afferents, by infecting tectal cells with a vaccinia virus (*22*) carrying the gene for a truncated calcium-calmodulin–independent form of CaMKII (tCaMKII) (*20*).

Morphological development of tectal neurons correlates well with position of the cell body along the RC axis (Fig. 1B), indicating that position along the RC axis can be used to select neurons at different stages of maturation. Whole-cell recordings were obtained from tectal neurons at different sites along the RC axis, and synaptic transmission was evoked by a stimulating electrode placed in the optic chiasm (Fig.

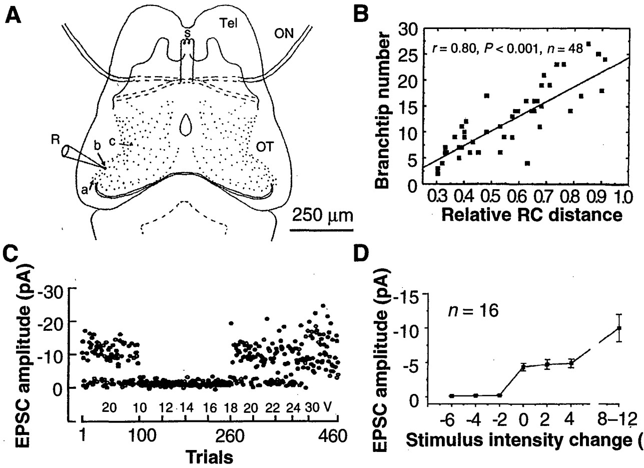

Fig. 1. (**A**) Diagram of the whole-brain preparation showing the stimulating electrode (S) in the optic chiasm and the recording patch-pipette (R) in the optic tectal cell body region (OT). Tel, telencephalon; ON, optic nerve. (**B**) Plot of dendritic branchtip number versus relative distance from the caudal border of the optic tectum. (**C**) EPSC amplitude does not change over a range of stimulus intensities above threshold, indicating single-fiber excitation. Plot of EPSC amplitude versus trials. Stimulus intensity was changed where indicated. (**D**) Ensemble average from 16 cells. The stimulus duration was varied (30 to 150 μs) so that threshold responses were obtained at about 20-V stimulus, indicated as 0 V on the *x* axis. After the threshold was set, voltage setting was changed (*x* axis) to determine response sensitivity to variations in stimulus intensity.

Cold Spring Harbor Laboratory, Cold Spring Harbor, NY 11724, USA.

*To whom correspondence should be addressed. E-mail: cline@cshl.org